Journal of the Brazilian Society of Mechanical Sciences and Engineering (2018) 40:551
https://doi.org/10.1007/s40430-018-1471-3

TECHNICAL PAPER

Optimization of a tuned liquid column damper subject to an arbitrary stochastic wind

Mansour H. Alkmim[1] · Adriano T. Fabro[1] · Marcus V. G. de Morais[1]

Received: 27 April 2018 / Accepted: 24 October 2018 / Published online: 3 November 2018

Abstract
The current Brazilian energy scenario is undergoing impactful changes. There is a clear need to adjust the current energy sector that presents an imbalance due to the almost exclusively dependency on hydroelectric power. This brings the need of diversifying the Brazilian energy matrix, including other energy sources that are both efficient and renewable. Amongst the available options, the wind energy stands out. Remarkable progress in wind turbine technology has been made over the past years, allowing the design of higher and slender structures for increasing efficiency in energy production. Parameter optimization for tuned liquid column dampers (TLCD), a class of passive structural control, has been previously proposed in the literature for reducing vibration in wind turbines and several other applications. However, most of the available work considers the wind excitation as either a deterministic harmonic load or random load with white noise spectra, which might not be representative of the actual wind load. This paper proposes an optimization approach for the TLCD parameters subjected to an arbitrary wind spectrum, given that its power spectral density is know. Finally, a numerical example is given in which a simplified wind turbine model is loaded by different stochastic wind profiles. Satisfactory reduction in the response vibration levels is found, and it is shown that different wind profiles can significantly affect the optimization results, i.e. the best TLCD parameters are dependent on the wind model.

Keywords Vibration suppression · Parameter optimization · Generalized pattern search · Random vibration analysis · TLCD

1 Introduction

The current Brazilian energy scenario is undergoing impactful changes. There is a clear need to adjust the current energy sector that presents an imbalance. Brazil depends almost exclusively on hydroelectric power. According to data released by PNE 2030 (National Energy Plan), most of the energy produced in the country comes from hydroelectric plants. By the year 2030, it is expected that hydroelectric plants will have a share of 77.4% of the energy matrix [30]. Since there is a need to diversify the Brazilian energy matrix, other energy sources that are efficient and renewable are sought. Amongst the possible options that stand out, wind and solar energy have been considered as important alternatives due to good geographical and economic conditions [11].

Wind turbines are structures that convert the mechanical movement generated by the force of the winds into electric energy. The wind reaches the rotor blades that transfer the rotational motion to an electric generator responsible for producing electricity. The increasing height of wind turbine also increases the need of new approaches to ensure structural reliability. Concerns over the integrity of wind turbines throughout the years have become a key point during design phase. The advance of the technology in wind turbines has caused an increase in its size and efficiency. In this way, challenges arise to avoid excessive vibration of both propellers and towers [5]. Higher and slender structures pose challenges concerning their integrity due to the dynamic loads from wind, ocean waves, or earthquakes [26]. Serious efforts have been undertaken to develop the concept of vibration control of wind turbines.

Technical Editor: Marcelo A. Trindade.

✉ Adriano T. Fabro
fabro@unb.br

[1] Department of Mechanical Engineering, University of Brasilia, Brasília, DF 70910-900, Brazil

The reduction in vibration, with the purpose of increasing its lifespan, motivates the use of several passive or semi-active vibration control techniques. In that sense, Murtagh [26] applied a tuned mass damper to mitigate vibration in a wind turbine by modelling the dynamic interaction between three uniform rotating turbine blades and their supporting uniform tower. Also, Zuluaga [43] investigated a tuned pendulum-shape mass damper to evaluate the reduction in displacement when the main system is subject to random ambient excitation. Lackner and Rotea [19] incorporated the equation of motion of the Tuned Mass Damper in the source code of FAST, an aero-elastic code. This scheme creates a more realistic model for structural control in wind turbines to significantly improve system's response. Li et al. [21] investigated experimentally the efficiency of a ball vibration absorber tested on a 1 / 13 scaled wind turbine. Fitzgerald and Basu [12] examined the effect of soil structure interaction on vibration control techniques. Zuo et al. [44] proposed the use of multiple tuned mass damper to control tower vibration of wind turbine by taking into consideration high vibrations modes.

Particularly, the use of tuned liquid column dampers (TLCD), first proposed by [22, 32], is a very attractive approach due to its relatively low cost and good efficiency [9, 23]. Recently, experimental investigations have been showing the potential of this approach in vibration mitigation of tall and slender structures [3, 6, 7, 42]. The main advantages of TLCD are its low cost, low maintenance frequency and multi-use of the device, e.g. water tank. Besides that, the TLCD does not require any bearings, special floor type for installation, activation of the mechanism, springs, and other mechanical elements that only increase the price of vibration absorber expenses. Consequently, their geometry varies according to design needs, making them quite versatile devices.

TLCDs were first studied for excitation of structures that underwent wind actions by [40]. The structure was modelled as a lumped mass multi-degree-of-freedom system taking into account both bending and shear, and the wind turbulence was modelled as a stochastic process that is stationary in time and non-homogeneous in space. The nonlinear damping term in the fundamental equation of the tuned liquid damper is treated by an equivalent linearization technique.

As shown in Fig. 1, TLCD operates based on the movement of the liquid column. The column may have different geometries; particularly in this paper, the TLCD has a "U" shape. The TLCD requires no extra mechanism such as springs or joints; furthermore, its geometry may vary according to design needs, making them very versatile devices. While the apparent simplicity of the system, its damping is dependent on the amplitude of the liquid column, making it a nonlinear problem.

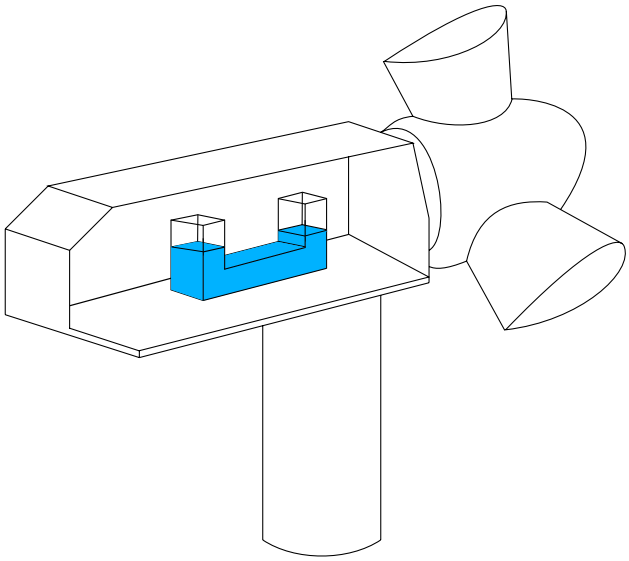

Fig. 1 Tuned liquid column damper scheme applied in a wind turbine [2]

The existence of a nonlinear term in the TLCD equation of motion is a drawback. Some approaches to simplify it have been proposed. Roberts and Spanos [31] have used a statistical linearization to avoid solving the nonlinear system of equations, and Vanderplaats [37] used a parameter optimization technique. A close form solution for the optimized TLCD damping ratio and head loss coefficient have been proposed by Yalla and Kareem [41]. The method does not rely on iterative process, but to solve the minimum variance integrals, an expression is derived indirectly considering some properties of the spectrum of the stationary output of a linear time-invariant system to white noise input. More recently, Altay et al. [2] presented an expanded optimization approach which considers the geometric layout of the damper. Numerical verification was carried out by stochastic inflow turbulence simulator TurbSim [28] and the aero-elastic dynamic horizontal axis wind turbine simulator FAST [29], which are well-known wind turbine simulation tools.

The goal of this paper is to attempt a more general optimization scheme that allows the search for optimum parameters of a TLCD for any stochastic wind model, given that its power spectral density is known. The structure of the paper starts by the mathematical description of TLCD and the wind turbine model in Sect. 2. A brief review on random vibration analysis of linear systems is presented in Sect. 3 followed by the proposed optimization approach. As a proof of stake, four different stochastic wind models and their effects on the optimum parameters are investigated in Sect. 5. Section 6 presents a numerical examples with the optimum parameters for the given wind load model, and finally, Sect. 7 presents some concluding remarks and further steps of the work.

2 TLCD and structure modelling

Considering the TLCD rigidly connected on the primary structure, as sketched in Fig. 2, and the "U"-shaped support with constant cross section and negligible mass when compared to fluid, it is possible to model the TLCD as a one-degree-of-freedom model with equivalent mass, stiffness and damping.

The equation describing the motion of the fluid is given by [34]

$$\rho A l\ddot{u}(t) + \frac{1}{2}\rho A\xi|\dot{u}(t)|\dot{u}(t) + 2\rho A g u(t) = -\rho A b\ddot{x}(t), \tag{1}$$

where $u(t)$ is the displacement of fluid, $x(t)$ is the displacement of the primary system, ρ is the fluid density, ξ is the head loss coefficient, A is the cross section area of the column, b and l are the horizontal and total length of the column, respectively, D is the diameter of the column, and g is the gravity constant. The TLCD equivalent mass, damping and stiffness are given, respectively, by $m_a = \rho A l$, $c_a = \frac{1}{2}\rho A\xi|\dot{u}(t)|$ and $k_a = 2\rho A g$. Therefore, the linearized column's natural frequency is given by $\omega_a = \sqrt{2g/l}$. The term on the right side of Eq. (1) is the coupling term with the primary structure.

The equation of motion of the primary structure is given by

$$(m_e + m_a)\ddot{x}(t) + \rho A b\ddot{u}(t) + c_e\dot{x}(t) + k_e x(t) = F(t), \tag{2}$$

where the parameter m_e is the structure mass, k_e the structure stiffness, c_e the structure damping, and $F(t)$ the excitation force. The term $\rho A b\ddot{u}(t)$ is a reaction force that occurs due to the motion of the liquid column induced by the structure. Thus, combining Eqs. (1) and (2), the equation of motion in matrix form is given by

$$\mathbf{M}\ddot{\mathbf{x}} + \mathbf{C}\dot{\mathbf{x}} + \mathbf{K}\mathbf{x} = \mathbf{f}, \quad |u| \leqslant \frac{l-b}{2}, \tag{3}$$

where

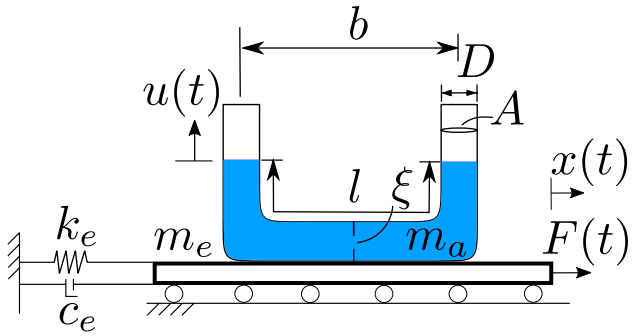

Fig. 2 Schematic model of TLCD rigidly connected to the primary structure

$$\mathbf{M} = \begin{bmatrix} m_e + m_a & \alpha m_a \\ \alpha m_a & m_a \end{bmatrix}, \quad \mathbf{C} = \begin{bmatrix} c_e & 0 \\ 0 & c_a \end{bmatrix},$$
$$\mathbf{K} = \begin{bmatrix} k_e & 0 \\ 0 & k_a \end{bmatrix}, \qquad \mathbf{f} = \begin{Bmatrix} F(t) \\ 0 \end{Bmatrix} \tag{4}$$

$\mathbf{x} = \{x\ u\}^T$, and $\alpha = b/l$ is the dimensionless length ratio. The condition presented by Eq. (3) is needed to ensure the liquid in the column does not spill over and consequently maintains its equivalent mass and damping characteristics. Additionally, Eq. (3) can also be written with the mass matrix in its dimensionless form, i.e.

$$\mathbf{M} = \begin{bmatrix} 1+\mu & \alpha\mu \\ \alpha & 1 \end{bmatrix}, \quad \mathbf{C} = \begin{bmatrix} 2\omega_e\zeta_e & 0 \\ 0 & \frac{\xi|\dot{u}|}{2l} \end{bmatrix},$$
$$\mathbf{K} = \begin{bmatrix} \omega_e^2 & 0 \\ 0 & \omega_a^2 \end{bmatrix}, \qquad \mathbf{f} = \begin{Bmatrix} \frac{F(t)}{m_e} \\ 0 \end{Bmatrix} \tag{5}$$

where ζ_e and ω_e are the damping ratio and natural frequency of the linearized structure, respectively. The dimensionless parameters mass ratio μ and tuning ratio γ are defined as $\mu = m_a/m_e$ and $\gamma = \omega_a/\omega_e$. It can be noticed that the nonlinear term is included in the damping matrix.

Murtagh at al. [25] presented a simplified model of wind turbine, assuming it as a cantilever beam such that the blade effects are negligible. This assumption is accurate for low-frequency analysis [15]. Then, system can be reduced to a single degree of freedom (DOF), with equivalent mass and equivalent stiffness of the tower given by [4]

$$k_e = \frac{\pi^4}{32L^3}EI, \tag{6}$$

$$m_e = \frac{mL}{2\pi}\left[\pi\left(3 + 2\frac{L_e}{L}\right) - 8\right], \tag{7}$$

where m is the mass per length of the beam, and E and I are the modulus of elasticity and the second moment of area, respectively. The tower length is given by L, and the equivalent tower length L_e is defined as $L_e = M/m$ where M is the equivalent lumped mass at the top of the cantilever beam.

2.1 Statistical linearization

The nonlinear nature of TLCD damping in Eq. (3) requires the determination of its equivalent form in order to perform random vibration analysis. Statistical linearization is the classical approach, but other methods can also be used. In this section, the linearization is firstly introduced followed by the parameter optimization.

Roberts et al. [31] proposed a procedure to estimate the linearized equivalent damping using statistical linearization.

From this approach, the error between the nonlinear term with its equivalent linearized can be expressed as $\varepsilon = \xi|\dot{u}|/2l - c_{\text{eq}}\dot{u}$, where the value of the equivalent damping c_{eq} can be obtained by minimizing the standard deviation of the error value, namely $E\{\varepsilon^2\}$. Assuming a probability density function with Gaussian form, it is possible to obtain an expression for the equivalent linearized damping as a function of the standard deviation of the fluid velocity $\sigma_{\dot{u}}$ and the head loss coefficient ξ. An iterative method is then carried out to find the optimized head loss coefficient.

Another linearization strategy is described in Yalla and Kareem [41]. By writing the TLCD's nonlinear damping in its linear form, $2\omega_{\text{a}}\zeta_{\text{a}}$, where ω_{a} and ζ_{a} are the TLCD's natural frequency and damping ratio, respectively, Yalla and Kareem minimized the primary structure variance response with respect to the damping ratio and the tuning ratio to find their optimal conditions when both equations were solved simultaneously. Although this method does not rely on iterative procedure, it involves a rather large computation [31]. Furthermore, the minimization solution changes if different wind models are used.

In this work, the proposed method considers the linearization as described in Yalla and Kareem [41] but rather than solving the optimization problem analytically, a numerical approach is considered. We can write Eq. (3) in its linearized form by changing its normalized damping matrix, Eq. (5), to

$$\mathbf{C} = \begin{bmatrix} 2\omega_{\text{e}}\zeta_{\text{e}} & 0 \\ 0 & 2\omega_{\text{a}}\zeta_{\text{a}} \end{bmatrix}. \tag{8}$$

From the linearized system, a frequency response function (FRF) is calculated which will be used in the random vibration analysis. The frequency response functions are obtained by assuming the system in Eq. (8) is under harmonic motion. The system response vector is then given by

$$\begin{aligned} \mathbf{X}(\omega) &= [-\omega^2\mathbf{M} + j\omega\mathbf{C} + \mathbf{K}]^{-1}\mathbf{F}(\omega) \\ &= \mathbf{H}(\omega)\mathbf{F}(\omega) \end{aligned} \tag{9}$$

where ω stands for the driving frequency, $\mathbf{F}(\omega)$ is the vector of the exciting force, $\mathbf{H}(j\omega) = [-\omega^2\mathbf{M} + j\omega\mathbf{C} + \mathbf{K}]^{-1}$ is the FRF, j is the imaginary unit, and $\mathbf{M}$, $\mathbf{C}$ and $\mathbf{K}$ are the mass, damping and stiffness matrix, respectively. For both degrees of freedom, the explicit expressions of the diagonal terms of the FRF matrix are given by

$$\begin{aligned} H_{11} &= \frac{(j\omega)^2 + \zeta_{\text{a}}\omega_{\text{a}}(j\omega) + \omega_{\text{a}}^2}{\Delta_H}, \\ H_{22} &= \frac{-\alpha(j\omega)^2}{\Delta_H}, \end{aligned} \tag{10}$$

where $\Delta_H = [(j\omega)^2(1+\mu) + 2\zeta_{\text{e}}\omega_{\text{e}}(j\omega) + \omega_{\text{e}}^2][(j\omega)^2 + 2\zeta_{\text{a}}\omega_{\text{a}}(j\omega) + \omega_{\text{a}}]^2 - (j\omega)^4\alpha^2\mu$. Equation (10) depends on the system parameters such as the absorber damping ratio and the natural frequencies.

3 Random vibration analysis

In this section, the random vibration analysis to find the system response in the frequency domain is introduced and some fundamental concepts are briefly reviewed. Expressions for the statistics of the random response, e.g. mean value, standard deviation and autocorrelation, of a linear systems under random stationary excitation can be given straightforwardly. However, nonlinear systems usually require the direct time domain solution of the differential equations in order to calculate the response statistics. Alternatively, a linearization method can be applied. When the systems are subjected to a deterministic load, a Taylor expansion around same equilibrium point is typically employed. For stochastic load, a statistical linearization scheme can be used, as shown in Sect. 2.1. Both, direct integration and linearization approaches, are summarized in the diagram shown in Fig. 3.

The equivalent linear approach is indicated by the upper path of the diagram, and load spectrum $S_{ff}(\omega)$ can be used directly to calculate the response spectrum $S_{yy}(\omega)$. The FRF $H(\omega)$ is given using the parameters obtained from the statistical linearization and is then used in the proposed procedure to calculate the optimized parameters.

The frequency content of a random process $x(t)$ is not periodic and therefore cannot be expressed by the Fourier series and also due to the stochastic nature of $x(t)$ that change from sample to sample. This difficulty in describing the process

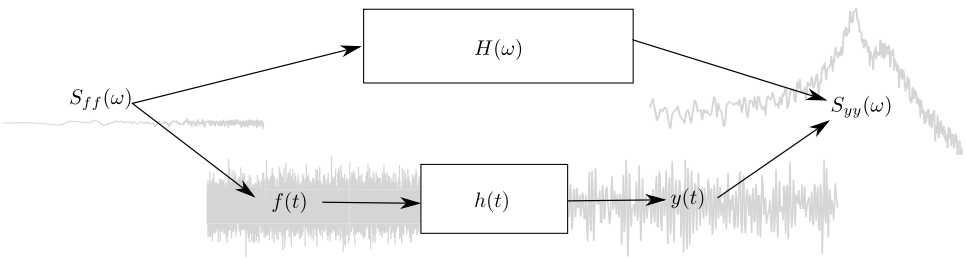

Fig. 3 Response PSD $S_{yy}(\omega)$ obtained from frequency response function for the linearized case (upper path), and from numerical integration for the nonlinear case (lower path)

can be solved by looking at the autocorrelation function $R_x(\tau)$ instead of the random function. $R_x(\tau)$ is a deterministic quantity and can be used to fully specify a zero-mean second-order stochastic process [38], and for a stationary random process, the autocorrelation function $R_{xx}(\tau)$ depends only on the time intervals, or lags, τ, regardless of the instant t. Additionally, from the autocorrelation function, it is possible to obtain information about the frequency content of a random process because it is related to the power spectral density (PSD) function of a stochastic process. The PSD is also a deterministic function and can be defined by the Fourier transform of the autocorrelation function as

$$S_{xx}(\omega) = \frac{1}{2\pi}\int_{-\infty}^{\infty} R_{xx}(\tau)e^{-i\omega\tau}\mathrm{d}\tau. \tag{11}$$

Consequently, it is possible to define the following relation

$$R_{xx}(\tau) = \int_{-\infty}^{\infty} S_{xx}(\omega)e^{i\omega\tau}\mathrm{d}\omega, \tag{12}$$

also known by Wiener–Khintchine theorem [27].

One of the particularly relevant properties of $S_{xx}(\omega)$ becomes apparent when $\tau = 0$ in Eq. (12); in this case,

$$E[x^2] = R_{xx}(\tau = 0) = \int_{-\infty}^{\infty} S_{xx}(\omega)\mathrm{d}\omega \tag{13}$$

where $E[\cdot]$ stands for the mathematical expectation. This result can be interpreted graphically, meaning that the mean squared of the random process is equal to the area under the spectral density curve.

The relation between the PSD of the response and the excitation can be extracted from the input and output ratios of a deterministic linear system. Let the elements $x(t)$ and $y(t)$ be the input and output of the system. Now, consider these functions in the frequency domain, $X(\omega)$ and $Y(\omega)$, and the relation between them can be obtained as

$$y(t) = \int_0^{\infty} h(\nu)x(t-\nu)\mathrm{d}\nu \xrightarrow{\mathfrak{F}} Y(\omega) = H(\omega)X(\omega), \tag{14}$$

where $\mathfrak{F}$ stands for Fourier Transform. Now, consider that $x(t)$ e $y(t)$ represent stochastic processes. The relations between input and output are still valid, but due to their stochastic nature there is the need to interpret these results in terms of theirs statistics, which are not deterministic quantities.

For the case where $x(t)$ is stationary, it can be shown that

$$R_{yy}(\tau) = \int_{-\infty}^{\infty}\int_{-\infty}^{\infty} h(\nu_1)R_{xx}(\tau+\nu_1-\nu_2)h^T(\nu)\mathrm{d}\nu_1\mathrm{d}\nu_2. \tag{15}$$

Applying the Fourier transform yields

$$S_{yy}(\omega) = S_{xx}(\omega)\int_{-\infty}^{\infty} h(\nu_1)e^{i\omega\nu_1}\mathrm{d}\nu_1\int_{-\infty}^{\infty} h^T(\nu_2)e^{-i\omega\nu_2}\mathrm{d}\nu_2, \tag{16}$$

which, using the definition of the impulse response function, leads to

$$S_{yy}(\omega) = |H(\omega)|^2 S_{xx}(\omega). \tag{17}$$

These results provide a direct and simple relation between the input and output power spectral density. Additionally, it is straightforward to generalize this results for systems with multiple DOF [27], yielding

$$S_{yy}(\omega) = \mathbf{H}(\omega)S_{xx}(\omega)\mathbf{H}(\omega)^T. \tag{18}$$

This is computationally more efficient than the direct time domain integration approach because a FFT-based approach can be used to estimate the input PSD [27, 33].

The direct integration in the time domain, typically requires the use a 4th-order Runge–Kutta–Fehlberg solver. The wind profile time history can be given from the wind PSD model $S_{ff}(\omega)$, further described in Sect. 5.1. Finally, the response PSD $S_{yy}(\omega)$ can be estimated via a periodogram approach [27]. Any optimization problem set find the best TLCD parameters according to a performance function, would require several evaluations of this nonlinear system and the same number of evaluations of the statistics of the response, which could be computationally prohibitive. A comparison between the two approaches was carried out in [1] where it was shown a good approximation between them.

4 Parameter optimization criteria

Assuming an external load $\mathbf{F}(t)$ as a stationary random signal with PSD given by $S_{ff}(\omega)$, the structural response $y(t)$ is also a stationary stochastic process with $S_{yy}(\omega)$ given by Eq. (18). Note that $S_{ff}(\omega)$ is proportional to the power spectral density of the wind velocity, and it can assume different models depending on the wind profile.

The desired performance index (cost function) J will be defined by the mean square response. If the exciting force is zero mean, then the response also has zero mean. Therefore, the mean square response Eq. (13) equals the variance, and thus

$$\begin{aligned} J(\zeta_a, \gamma) &= \int_{-\infty}^{\infty} S_{yy}(\omega)\mathrm{d}\omega \\ &= \int_{-\infty}^{\infty} \mathbf{H}(\omega)S_{ff}(\omega)\mathbf{H}(\omega)^T\mathrm{d}\omega, \end{aligned} \tag{19}$$

where the response PSD $S_{yy}(\omega)$ is real positive and, therefore, the sufficient and necessary conditions for the optimization are met [20]. For the prescribed frequency range $[\omega_l, \omega_u]$ the optimization problem consists of looking for the parameters that minimize the area under of response PSD over a given frequency band, i.e.

$$\begin{aligned} &\min_{\zeta_a,\gamma\in\Omega} J_i(\zeta_a,\gamma) \\ s.t. \quad &\zeta_a,\gamma \geq 0 \\ I = \{i \mid &\omega_l \leq \omega_i \leq \omega_u\} \end{aligned} \tag{20}$$

where Ω is the set of design parameters TLCD damping ratio ζ_a and tuning ratio γ satisfying the constraint. To solve the optimization problem, we introduce the optimization algorithm in the next subsection.

4.1 Generalized patter search

The Generalized Patter Search (GPS) is a class of direct search methods, and it was originally proposed for unconstrained minimization problems [14] and then extended for problems with bound and linear constraints [36]. The classical gradient-based algorithms have they performance strongly affected when the cost function includes some random noise. Although the GPS requires more function evaluations than gradient-based algorithms to find the true minimum, it is not as strongly affected by random noise [17].

The function *patternsearch* from the MATLAB environment is used as a GPS implementation. Algorithm 1 is applied in this work for the proposed parameter optimization problem.

Algorithm 1 *patternsearch* algorithm

```
X0 = [zeta gamma];          # Starting point
LB = [0 0];                   # Lower bound
UB = [inf inf];               # Upper bound
Objfcn = @objfun;
PSoptions = optimoptions('patternsearch',...
                         'ConstraintTolerance',1e-14,
                         'FunctionTolerance',1e-14,
                         'StepTolerance',1e-14);
[xopt,Fps] = patternsearch(Objfcn,X0,[ ],[ ],[ ],[ ],LB,UB,PSoptions);
```

4.2 Verification procedure

In order to verify whether the algorithm and cost function are adequate for solving the optimization problem, a simple case where the closed-form solution is available is investigated.

Considering the case of undamped primary structure ($\zeta_e = 0$) and white noise excitation, Yalla and Kareem [41] solved the mean variance problem to obtain the following expression for optimal parameters

$$\zeta_{opt} = \frac{\alpha}{2}\sqrt{\frac{2\mu\left(\alpha^2\frac{\mu}{4} - \mu - 1\right)}{(\alpha^2\mu^2 + \alpha^2\mu - 4\mu - 2\mu^2 - 2)}}, \tag{21}$$

$$\gamma_{opt} = \frac{\sqrt{1 + \mu(1 - \frac{\alpha^2}{2})}}{1 + \mu}, \tag{22}$$

which are function of the length ratio α and mass ratio μ.

Figures 4 and 5 show the optimized parameters from Yalla and Kareem [41] and the proposed algorithm as a function of the mass ratio for different length ratio α. It can be noticed a very good agreement in Fig. 4. A slight difference in Fig. 5 can be seen between the two methods in the optimum damping ratio for large values of mass ratio which can be attributed to tolerance error in the optimization algorithm and the chosen cost function's interval of integration that, in this case, was chosen between 2 and 5 rad/s. However, the optimized damping ratio sensitivity does not influence the characteristics of the system.

The wind excitation PSDs considered in this paper are detailed in the next section.

5 Probabilist description of wind loads

This section summarizes some probabilistic aspects of wind load in low atmospheric layers on flexible structures. The problems is confined to along-wind response of structures, and cross-wind response or aero-elastic coupled problems are not in the scope of this work and are therefore left out of discussion.

The wind velocity fluctuates as a function of the time near the ground. In fact, the spectral analysis of this velocity over a long time interval reveals several scales of fluctuation. Figure 6 shows the van der Hoven spectrum [18], a typical power spectrum of the horizontal velocity

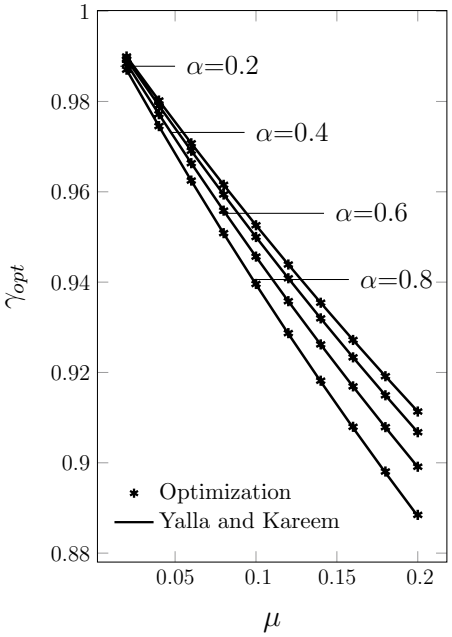

Fig. 4 Optimized tuning ratio subject to white noise spectrum as a function of the mass ratio μ for different length ratio α

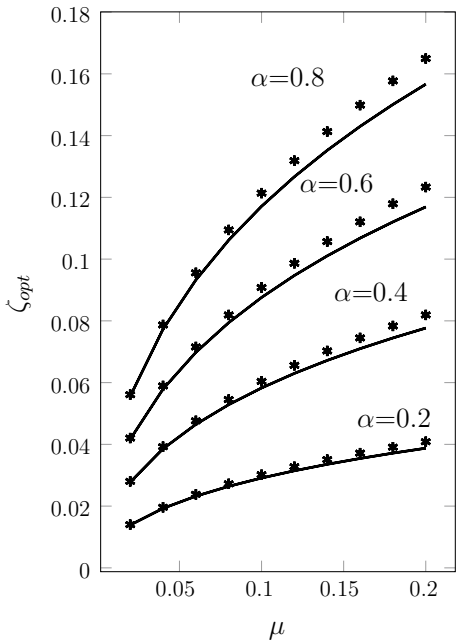

Fig. 5 Optimized damping ratio subject to white noise spectrum as a function of the mass ratio μ for different length ratio α

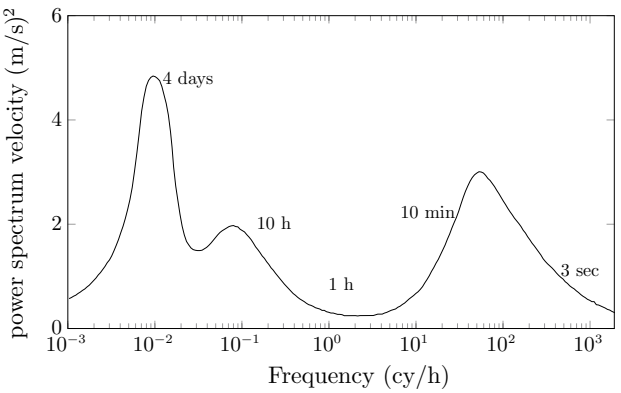

Fig. 6 The van der Hoven power spectrum of the horizontal velocity of wind at 100 m above the ground. Adapted from [18]

of wind at 100 metres above ground. It shows that the low-frequency energy is concentrated over a period of four days, which is associated with geostrophic motions. Another peak is commonly placed at 12 or 24 h and is due to thermal phenomena of night and day alternation. For last, part of the energy is concentrated over a period of one minute and corresponds to the timescale of turbulent motion. These micro-meteorological effects can be attribute to turbulent gust caused by eddies in the wind load over obstacles in the vicinity of the turbine, i.e. towns, trees, hills and valleys. If the surface is relatively flat such as in the sea, there will be less turbulence then in the field.

The effects of coupling of the wind velocity with the structural motion can be neglected, and therefore the wind load can be given only by the wind velocity, which can be divided into static and dynamic components. Moreover, both along-wind and across-wind load directions can be considered separately [39]. Wind turbulence is an important consideration if the first natural period of a structure is around 0.5 s and it is mostly likely the cause of fatigue damage in lattice towers [13]. The power spectrum from Fig. 6 also shows that there is an energy hole for periods between 10 min and 2 h. Therefore, if an average wind velocity is desirable over a period T corresponding to the energy hole, i.e. in the 10 min up to 2 h range, the mean velocity will be almost stable [18] and over a time T the wind velocity can be modelled by a locally stationary stochastic process.

Two approaches can follow, a short-term and a long-term modelling. The short-term modelling describes the fast fluctuations due to turbulence and is modelled by a stochastic process. If we take into account the slow variations of the mean velocity over a long period, we obtain a long-term modelling. However, due to lack of meteorological deterministic forecast over a long period, one has to resort to probabilistic modelling. Hence, the mean velocity and other parameters are modelled by random variables where the probabilistic models are the outcome of statistical processing of meteorological measurements.

The analysis in this work focuses on the short-term model for wind flow, and the following section will describe typical PSD profiles used to model stochastic wind load.

5.1 Wind profile power spectral density

Wind excitations are highly dynamic, irregular external loads. This section discusses how these could be simulated through the different PSDs such as white noise, Kanai–Tajimi, Kaimal and Davenport.

White noise is a signal idealization where its PSD covers all frequency bands with a constant value. Other PSD models can be physically more meaningful to represent wind profiles by taking into account aspects of relevance to the real problem such as roughness, heights, wind forces and general changes in dynamic properties. Kaimal and Davenport spectrum models are a first-order filter that can be used to approximate wind-induced positive pressures along wind loading. Kanai–Tajimi is a representation of a second-order filter, which is typically used in earthquake profiles, but will be used in this work for the sake of comparison. Table 1 summarizes each respective power spectral density function expressions.

For Kaimal PSD, $L_k = 340.2$ m is a scale parameter that involves the wind turbine high and $v_{hub} = 16$ m/s is the mean wind velocity. According to Burton et al. [8], Kaimal spectrum provides a good fit to empirical observation of

Table 1 Power spectral density functions for modelling the wind

Filter	Power spectral density functions
White noise	$S_{\mathrm{WN}}(\omega) = S_0$
Kanai–Tajimi	$S_{\mathrm{KT}}(\omega) = \frac{(1+4\xi_g^2(\omega/\omega_g)S_0)}{[1+(\omega/\omega_g)^2+4\xi_g^2(\omega/\omega_g)^2]}$
Kaimal	$S_{\mathrm{Kai}}(\omega) = \left[\frac{4S_0^2(L_k/v_{\mathrm{hub}})}{[1+(6\omega(L_k/v_{\mathrm{hub}}))}\right]^{5/3}$
Davenport	$S_{\mathrm{Dav}}(\omega) = \frac{4\kappa L v_{\mathrm{hub}}^2 \chi}{(1+\chi^2)^{4/3}}, \quad \chi = \omega L/v_{\mathrm{hub}}$

atmospheric turbulence. For Davenport PSD, κ is the drag coefficient referred to the mean velocity and L in the hub height [10]. For Kanai–Tajimi PSD, $\omega_g = 10.5$ rad/s and $\xi_g = 0.317$ can be interpreted as characteristic frequency and characteristic damping ratio, respectively [16]. Kanai–Tajimi spectrum amplifies the frequency around ω_g and it attenuates high frequencies [35].

Figures 7 and 8 show the spectral and time history characteristics of different wind models with added Gaussian noise, respectively. From Fig. 7, it can be noticed that both Kaimal and Davenport spectra show more dominant low-frequency components. Since Kanai–Tajimi is a second-order filter, the formation of a peak near its characteristic frequency can be clearly noticed. In addition, Fig. 8 shows the velocity of the wind in the time domain. This time history is numerically

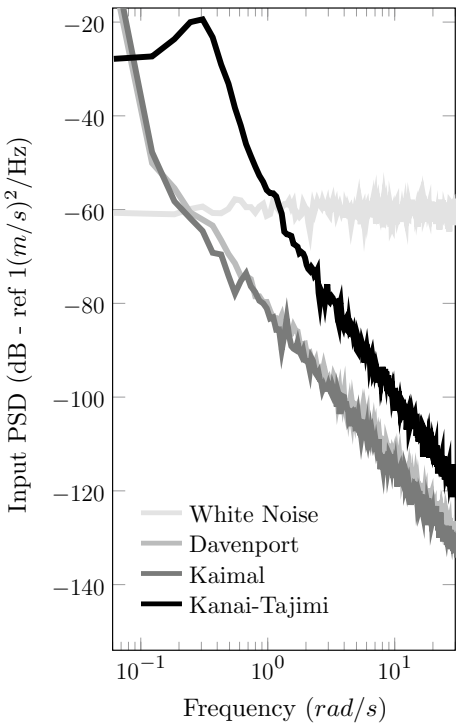

Fig. 7 Power spectral density of the wind velocity for white noise, Davenport, Kaimal and Kanai–Tajimi models

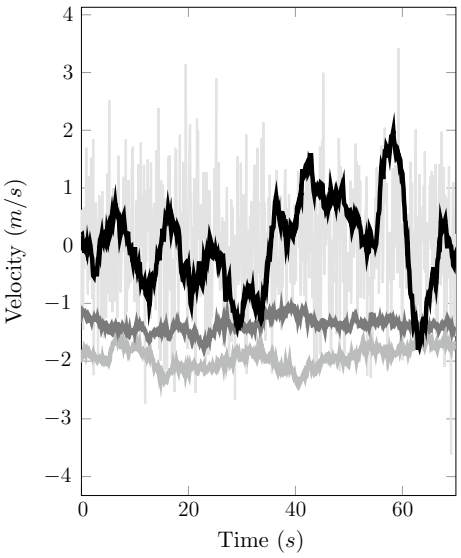

Fig. 8 Zero-mean time history of the wind velocity for white noise, Davenport, Kaimal and Kanai–Tajimi models

generated by a FFT-based algorithm, taking the inverse discrete Fourier transform (IDFT) of the discretized signal in the frequency domain where its amplitude is estimated as the square root of the discretized PSD, $\sqrt{S_k}$, and the random phase is generated from a uniform distribution within the interval $[0, 2\pi]$ [27].

It can be noticed that the white noise velocity profile is the least smooth of all, because the velocity at one point in time is independent from the velocity at any other instant. Moreover, it has the largest dispersion around the mean which is proportional to the area under the PSD curve. This spectral is not physically meaningful, but it is usually applied because it is easier to manipulate analytically than other model. The Kanai–Tajimi spectrum also shows a large dispersion, due to its large area under the PSD curve, but it presents smoother time domain history than the white noise spectrum. Finally, Kaimal and Davenport spectra present a more physically meaningful wind velocity profile with good autocorrelation [24].

The next section describes a numerical example using random vibration analysis, the described wind profiles and the parameters obtained from the optimization approach.

6 Numerical example

In this section, a numerical example is carried out using the wind turbine parameters, summarized in Table 2, which are the same as proposed by Murtagh et al. [25]. First, optimized parameters are obtained for a fixed length ratio and different mass ratios and wind spectra cases. Then, comparisons

of the system response PSD with and without TLCD are shown.

Table 3 presents the obtained optimized TLCD damping ratio ζ_{opt} and tuning ratio γ_{opt} for a fixed length ratio $\alpha = 0.8$ and different mass ratio and wind spectra. Fixed length ratio configuration is chosen because both mass and length ratios are inversely proportional and related to the physical constraint horizontal length of the liquid column b as follows

$$\mu = \left(\frac{\rho A}{m_{\text{e}}}\right)\frac{b}{\alpha}. \tag{23}$$

where a fixed length ratio can have different horizontal b lengths for each mass ratio.

From Table 3, it can be seen that the optimum TLCD damping ratio ζ_{opt} increases for increasing mass ratio μ, and it is only slightly affected by the choice of wind spectrum. This can be clearly noticed from Fig. 9. On the other hand, the optimum tuning ratio γ_{opt} decreases for increasing mass ratio μ and it is significantly affected by the choice of wind spectrum, as can be clearly seen from Fig. 10. Kaimal and Davenport spectra present almost the same values of tuning ratio, which are overall increasingly smaller for increasing mass ratio μ, when compared to the white noise spectrum. This is expected, since both Kaimal and Davenport spectra are very similar to each other and with significantly more energy content in lower frequencies, when compared to the white noise spectrum. Moreover, Kanai–Tajimi spectrum shows overall larger values of optimized tuning ratio. Furthermore, the choice of wind spectrum can influence the response magnitude and therefore it is relevant for the appropriate choice of optimum TLCD parameters.

Figures 11 and 12 show the system response in frequency and time domain, respectively, under Kaimal spectrum excitation and optimized parameters for $\mu = 0.06$. A significant reduction in the response is overall obtained in both PSD S_{yy} and time domain response, when compared to the case without TLCD, as expected. Moreover, results are shown for two other cases in which

Table 2 Wind turbine parameters

Parameter	Symbol	Equation	Value	Unit
Modulus of elasticity	E		2.1×10^{11}	Pa
Width	D		3	m
Thickness	t		0.015	m
Cross-sectional area	A	πDt	0.14	m^2
Steel density	ρ_s		7850	kg/m^3
Tip mass	M		19876	kg
Beam mass per length	m	$\rho_s A$	1110	kg/L
Total length	L		60	m
Equivalent length	L_{e}	M/m	17.91	
Second moment of area	I	$\pi t D^3/8$	0.16	m^4
Structure stiffness	k_{e}	Eq. (5)	470685	N/m
Structure mass	m_{e}	Eq. (6)	34975	kg
Structure natural frequency	ω_{e}	$\sqrt{k_{\text{e}}/m_{\text{e}}}$	3.67	rad/s
Structure damping ratio	ζ_{e}	$c_{\text{e}}/2m_{\text{e}}\omega_{\text{e}}$	1.83	%

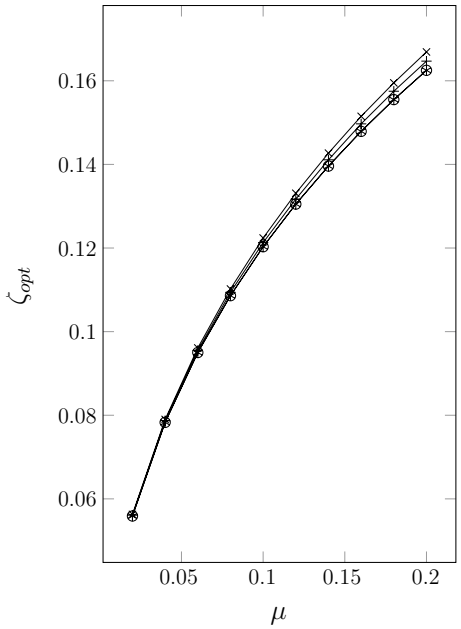

Fig. 9 Optimum damping ratio ζ_{opt} subject to different wind spectra as a function of the mass ratio μ for a fixed length ratio α=0.8 and 1% primary structural damping

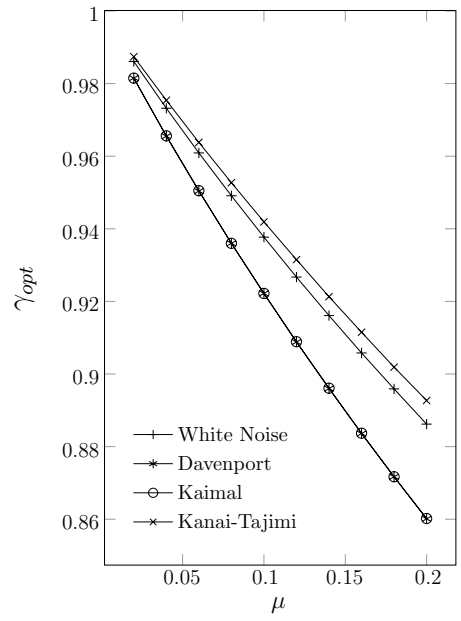

Fig. 10 Optimum tuning ratio γ_{opt} subject to different wind spectra as a function of the mass ratio μ for a fixed length ratio $\alpha = 0.8$ and 1% primary structural damping

Table 3 Optimized LCD damping ratio ζ_{opt} and tuning ratio γ_{opt} for a fixed length ratio $\alpha = 0.8$ and 1% primary structural damping

μ	White noise		Davenport		Kaimal		Kanai–Tajimi	
	ζ_{opt}	γ_{opt}	ζ_{opt}	γ_{opt}	ζ_{opt}	γ_{opt}	ζ_{opt}	γ_{opt}
0.02	0.0561	0.9861	0.0559	0.9815	0.0559	0.9815	0.0563	0.9874
0.04	0.0787	0.9732	0.0783	0.9655	0.0783	0.9656	0.0790	0.9754
0.06	0.0955	0.9609	0.0950	0.9504	0.0950	0.9505	0.0961	0.9638
0.08	0.1094	0.9491	0.1086	0.9360	0.1086	0.9360	0.1102	0.9527
0.10	0.1213	0.9377	0.1203	0.9222	0.1203	0.9222	0.1224	0.9419
0.12	0.1317	0.9267	0.1305	0.9088	0.1305	0.9089	0.1331	0.9315
0.14	0.1411	0.9161	0.1396	0.8960	0.1396	0.8961	0.1427	0.9213
0.16	0.1497	0.9058	0.1479	0.8836	0.1479	0.8837	0.1515	0.9115
0.18	0.1575	0.8959	0.1555	0.8717	0.1555	0.8717	0.1595	0.9019
0.20	0.1647	0.8862	0.1625	0.8601	0.1625	0.8602	0.1669	0.8927

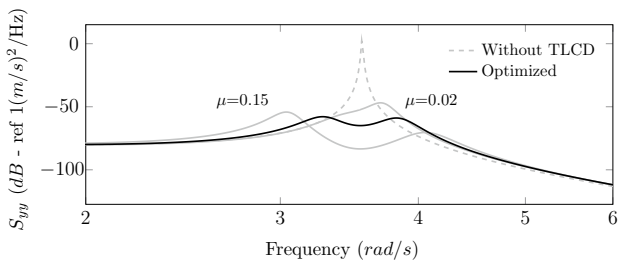

Fig. 11 Response of main system under Kaimal spectrum for $\mu = 0.06$ and $\alpha = 0.8$ without TLCD (dashed), optimized (solid black) and two different mass ratio (solid grey scale) in the frequency domain

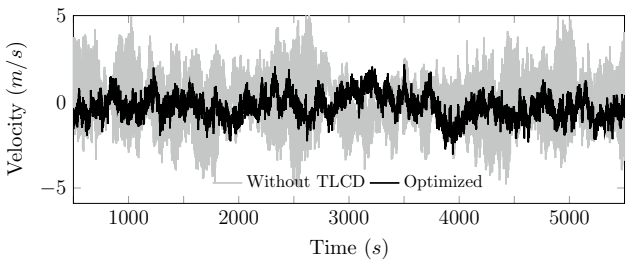

Fig. 12 Response of main system under Kaimal spectrum for $\mu = 0.06$ and $\alpha = 0.8$ without TLCD (solid grey scale) and optimized (solid black) in the time domain

non-optimum parameters are chosen for $\mu = 0.02$ and $\mu = 0.15$, to illustrate the effect of optimized parameters. Recall that the optimum performance is defined by the minimizing the area under the response PSD. The optimized response shows two peaks with same magnitude, the latter presents two peaks, one slightly bigger than the other and the former has only one peak, which is bigger than the optimized one. Note that results for different values of length ratio α would yield similar effects, since they are related by Eq. (23), due to the physical constraint horizontal length of liquid column.

7 Concluding remarks

This paper proposes a more general optimization scheme that allows the search for optimum parameters of a TLCD for a arbitrary stochastic wind model, given that its power spectral density is known. The TLCD model presents a nonlinear damping term due to the head loss coefficient. A statistical linearization approach is applied which considers the mean error between the nonlinear and linearized systems in a statistical sense.

An optimization criterion is chosen such that it minimizes the area under the response PSD S_{yy} and the use of a global direct search optimization algorithm is proposed to find optimum TLCD parameters. This strategy allows for finding the optimized parameters for a more general case such that an arbitrary wind model can be used. Four different wind models, given by a PSD profile, were investigated, namely Davenport, Kaimal, Kanai–Tajimi and a white noise. The numerical results show that the choice of the stochastic wind model can significantly affect the optimum TLCD parameters. The use of only white noise models, typically found in the literature, might give misleading results.

The TLCD design parameters can be given by its damping ratio ζ and tuning ratio γ. The optimum TLCD damping ratio ζ_{opt} increases for increasing mass ratio μ, and it is only slightly affected by the choice of wind spectrum. Besides, the optimum tuning ratio γ_{opt} decreases for increasing mass ratio μ and it is significantly affected by the choice of wind spectrum.

Finally, further work is necessary for model validation, including experimental validation and sensitivity analysis, and more complex models for the wind turbine, including higher-order modes and the effects of the turbine blades.

Acknowledgements The authors would like to thank CNPq and MCTI, process number 406895/2013-9, and FAPDF, process number 0193.001359/2016), for the financial support.

References

1. Alkmim MH, de Morais MVG, Fabro AT (2016) Vibration reduction of wind turbines using tuned liquid column damper using stochastic analysis. In: Journal of physics: conference series, vol 744. IOP Publishing, p 012178
2. Altay O, Butenweg C, Klinkel S, Taddei F (2014) Vibration mitigation of wind turbine towers by tuned liquid column dampers. In: Proceedings of the IX international conference on structural dynamics, Porto, Portugal, vol 12
3. Altuniik AC, Yetiken A, Kahya V (2018) Experimental study on control performance of tuned liquid column dampers considering different excitation directions. Mech Syst Signal Process 102:59–71. https://doi.org/10.1016/j.ymssp.2017.09.021
4. Avila SM, Barcelos M, Morais M, Shzu MA, Silva RdC (2009) Vibration control of the set tower and wind turbine under the wind influence. In: 20th international congress of mechanical engineering COBEM
5. Azevedo HDMd, Filho PHCdA, Arajo AM, Bouchonneau N, Rohatgi JS, Souza RMCd (2017) Vibration monitoring, fault detection, and bearings replacement of a real wind turbine. J Braz Soc Mech Sci Eng 39(10):3837–3848. https://doi.org/10.1007/s40430-017-0853-2
6. Bhattacharyya S, Ghosh AD, Basu B (2017) Nonlinear modeling and validation of air spring effects in a sealed tuned liquid column damper for structural control. J Sound Vib 410:269–286. https://doi.org/10.1016/j.jsv.2017.07.046
7. Buckley T, Watson P, Cahill P, Jaksic V, Pakrashi V (2018) Mitigating the structural vibrations of wind turbines using tuned liquid column damper considering soil-structure interaction. Renew Energy 120:322–341. https://doi.org/10.1016/j.renene.2017.12.090
8. Burton T, Sharpe D, Jenkins N, Bossanyi E (2001) Wind energy handbook. Wiley, Hoboken
9. Colwell S, Basu B (2009) Tuned liquid column dampers in offshore wind turbines for structural control. Eng Struct 31(2):358–368
10. Davenport AG (1961) The spectrum of horizontal gustiness near the ground in high winds. Q J R Meteorol Soc 87(372):194–211
11. De Jong P, Sánchez A, Esquerre K, Kalid RdA, Torres EA (2013) Solar and wind energy production in relation to the electricity load curve and hydroelectricity in the northeast region of brazil. Renew Sustain Energy Rev 23:526–535
12. Fitzgerald B, Basu B (2016) Structural control of wind turbines with soil structure interaction included. Eng Struct 111:131–151
13. Halfpenny A (1998) Dynamic analysis of both on and offshore wind turbines in the frequency domain. Ph.D. thesis, University of London
14. Hooke R, Jeeves TA (1961) Direct search solution of numerical and statistical problems. J ACM (JACM) 8(2):212–229
15. Kang N, Park SC, Park J, Atluri SN (2016) Dynamics of flexible tower-blade and rigid nacelle system: dynamic instability due to their interactions in wind turbine. J Vib Control 22(3):826–836
16. Kareem A (1984) Model for predicting the acrosswind response of buildings. Eng Struct 6(2):136–141
17. Kolda TG, Lewis RM, Torczon V (2003) Optimization by direct search: new perspectives on some classical and modern methods. SIAM Rev 45(3):385–482
18. Krée P, Soize C (2012) Mathematics of random phenomena: random vibrations of mechanical structures, vol 32. Springer, Berlin
19. Lackner MA, Rotea MA (2011) Passive structural control of offshore wind turbines. Wind Energy 14(3):373–388
20. Lee CL, Chen YT, Chung LL, Wang YP (2006) Optimal design theories and applications of tuned mass dampers. Eng Struct 28(1):43–53
21. Li J, Zhang Z, Chen J (2012) Experimental study on vibration control of offshore wind turbines using a ball vibration absorber. Energy Power Eng 4(03):153
22. McNamara RJ (1977) Tuned mass dampers for buildings. J Struct Div 103(9):1785–1798
23. Min KW, Kim J, Lee HR (2014) A design procedure of two-way liquid dampers for attenuation of wind-induced responses of tall buildings. J Wind Eng Ind Aerodyn 129:22–30
24. Murtagh P, Basu B, Broderick B (2004) Wind force time-history generation by discrete Fourier transform (dft). In: Multi-body dynamics: monitoring and simulation techniques III 3rd
25. Murtagh P, Basu B, Broderick B (2005) Along-wind response of a wind turbine tower with blade coupling subjected to rotationally sampled wind loading. Eng Struct 27(8):1209–1219
26. Murtagh P, Ghosh A, Basu B, Broderick B (2008) Passive control of wind turbine vibrations including blade/tower interaction and rotationally sampled turbulence. Wind Energy 11(4):305–317
27. Newland DE (2012) An introduction to random vibrations, spectral & wavelet analysis. Courier Corporation, New York
28. NWTC Information Portal (TurbSim) (2016) https://nwtc.nrel.gov/TurbSim. Accessed 26 April 2018
29. NWTC Information Portal (FAST) (2018) https://nwtc.nrel.gov/FAST. Accessed 26 April 2018
30. Pottmaier D, Melo C, Sartor M, Kuester S, Amadio T, Fernandes C, Marinha D, Alarcon O (2013) The Brazilian energy matrix: from a materials science and engineering perspective. Renew Sustain Energy Rev 19:678–691
31. Roberts JB, Spanos PD (2003) Random vibration and statistical linearization. Courier Corporation, New York
32. Sakai F, Takaeda S, Tamaki T (1989) Tuned liquid column damper-new type device for suppression of building vibrations. In: International conference on Highrise buildings, Nanjing, China, pp 25–27
33. Shin K, Hammond J (2008) Fundamentals of signal processing for sound and vibration engineers. Wiley, New York
34. Streeter VL, Wylie EB, Bedford KW (1998) Fluid mechanics, WCB. McGraw-Hill, Boston
35. Thráinsson H, Kiremidjian AS, Winterstein SR (2000) Modeling of earthquake ground motion in the frequency domain. In: John A, Blume Earthquake Engineering Center
36. Torczon V (1997) On the convergence of pattern search algorithms. SIAM J Optim 7(1):1–25
37. Vanderplaats GN (1984) Numerical optimization techniques for engineering design: with applications, vol 1. McGraw-Hill, New York
38. Vanmarcke E (2010) Random field: analysis and synthesis, 2nd edn. Word Scientific, Cambridge
39. Wu J, Yang J (1998) Active control of transmission tower under stochastic wind. J Struct Eng 124(11):1302–1312
40. Xu Y, Samali B, Kwok K (1992) Control of along-wind response of structures by mass and liquid dampers. J Eng Mech 118(1):20–39
41. Yalla SK, Kareem A (2000) Optimum absorber parameters for tuned liquid column dampers. J Struct Eng 126(8):906–915
42. Yu Y, Xu L, Zhang L (2017) Experimental study on variation rules of damping with influential factors of tuned liquid column damper. Shock Vib 2017:17. https://doi.org/10.1155/2017/6209205
43. Zuluaga AL (2007) Controle de vibração em edifícios submetidos à ação de carga dinâmicas utilizando amortecedor de massa sintonizado na forma de pêndulo. Master's thesis, University of Brasilia
44. Zuo H, Bi K, Hao H (2017) Using multiple tuned mass dampers to control offshore wind turbine vibrations under multiple hazards. Eng Struct 141:303–315